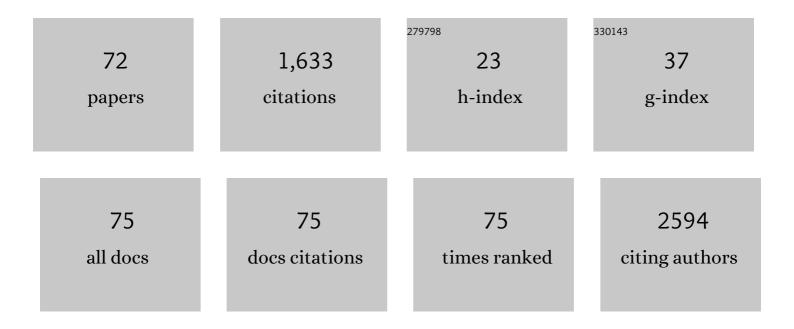
List of Publications by Year in descending order

Source: https://exaly.com/author-pdf/325736/publications.pdf Version: 2024-02-01



#	Article	IF	CITATIONS
1	Incidence rate and factors associated with the development of secondary cancers after radioiodine therapy in differentiated thyroid cancer: a multicenter retrospective study. European Journal of Nuclear Medicine and Molecular Imaging, 2022, 49, 1661-1670.	6.4	8
2	Clinical implication of minimal presence of solid or micropapillary subtype in earlyâ€stage lung adenocarcinoma. Thoracic Cancer, 2021, 12, 235-244.	1.9	23
3	Robustness of magnetic resonance radiomic features to pixel size resampling and interpolation in patients with cervical cancer. Cancer Imaging, 2021, 21, 19.	2.8	28
4	Value of accurate diagnosis for metastatic supraclavicular lymph nodes in breast cancer: assessment with neck US, CT, and 18F-FDG PET/CT. Diagnostic and Interventional Radiology, 2021, 27, 323-328.	1.5	0
5	Clinical impact of radioactive iodine dose selection based on the number of metastatic lymph nodes in patients with papillary thyroid carcinoma: A multicenter retrospective cohort study. Clinical Endocrinology, 2021, 95, 901-908.	2.4	1
6	Mapping patterns of para-aortic lymph node recurrence in cervical cancer: a retrospective cohort analysis. Radiation Oncology, 2021, 16, 128.	2.7	3
7	Favorable Long-Term Outcomes with Autologous Stem Cell Transplantation for High-Risk Multiple Myeloma Patients with a Positive Result On 18F-FDG PET/CT at Baseline. Clinical Lymphoma, Myeloma and Leukemia, 2021, , .	0.4	1
8	Prediction Model for Tumor Budding Status Using the Radiomic Features of F-18 Fluorodeoxyglucose Positron Emission Tomography/Computed Tomography in Cervical Cancer. Diagnostics, 2021, 11, 1517.	2.6	6
9	Direct Comparison of Preoperative Imaging Modalities for Localization of Primary Hyperparathyroidism. JAMA Otolaryngology - Head and Neck Surgery, 2021, 147, 692.	2.2	22
10	Prognostic impact of 18F-FDG PET/CT in patients with multiple myeloma presenting with renal impairment. International Journal of Hematology, 2021, 113, 668-674.	1.6	0
11	Predicting Tumor Budding Status in Cervical Cancer Using MRI Radiomics: Linking Imaging Biomarkers to Histologic Characteristics. Cancers, 2021, 13, 5140.	3.7	5
12	Development of a new risk stratification system for patients with newly diagnosed multiple myeloma using R-ISS and 18F-FDG PET/CT. Blood Cancer Journal, 2021, 11, 190.	6.2	10
13	On the Potential Benefit of Shunt Surgery in Idiopathic Normal-Pressure Hydrocephalus Patients with Alzheimer's Disease Pathology. Dementia and Neurocognitive Disorders, 2021, 20, 108.	1.4	1
14	White blood cell labeling with Technetium-99m (99mTc) using red blood cell extracellular vesicles-mimetics. Blood Cells, Molecules, and Diseases, 2020, 80, 102375.	1.4	15
15	Utility of 18F-FDG PET/CT for predicting pathologic complete response in hormone receptor-positive, HER2-negative breast cancer patients receiving neoadjuvant chemotherapy. BMC Cancer, 2020, 20, 1106.	2.6	11
16	Abnormal cortical thickening and thinning in idiopathic normal-pressure hydrocephalus. Scientific Reports, 2020, 10, 21213.	3.3	11
17	Assessment of betaâ€amyloid deposition using gray matter delineation by earlyâ€phase Fâ€18 florbetaben PET in patients with brain atrophy. Alzheimer's and Dementia, 2020, 16, e038717.	0.8	0
18	Abnormal thickening and thinning of the cerebral cortex in idiopathic normalâ€pressure hydrocephalus. Alzheimer's and Dementia, 2020, 16, e042212.	0.8	0

#	Article	IF	CITATIONS
19	Extracellular vesicles derived from macrophage promote angiogenesis In vitro and accelerate new vasculature formation In vivo. Experimental Cell Research, 2020, 394, 112146.	2.6	28
20	Improving the Prognostic Performance of SUVmax in 18F-Fluorodeoxyglucose Positron-Emission Tomography/Computed Tomography Using Tumor-to-Liver and Tumor-to-Blood Standard Uptake Ratio for Locally Advanced Cervical Cancer Treated with Concurrent Chemoradiotherapy. Journal of Clinical Medicine, 2020, 9, 1878.	2.4	2
21	A new tyrosine kinase inhibitor K905-0266 inhibits proliferation and sphere formation of glioblastoma cancer cells. Journal of Drug Targeting, 2020, 28, 933-938.	4.4	1
22	Comparison of 5 Different PET Radiopharmaceuticals for the Detection of Recurrent Medullary Thyroid Carcinoma. Clinical Nuclear Medicine, 2020, 45, 341-348.	1.3	36
23	Prognosis-Predicting Model Based on [18F]fluorodeoxyglucose PET Metabolic Parameters in Locally Advanced Cervical Cancer Patients Treated with Concurrent Chemoradiotherapy: Multi-Center Retrospective Study. Journal of Clinical Medicine, 2020, 9, 427.	2.4	10
24	A Novel Tyrosine Kinase Inhibitor Can Augment Radioactive Iodine Uptake Through Endogenous Sodium/Iodide Symporter Expression in Anaplastic Thyroid Cancer. Thyroid, 2020, 30, 501-518.	4.5	18
25	Magnetic resonance imaging features of tumor and lymph node to predict clinical outcome in node-positive cervical cancer: a retrospective analysis. Radiation Oncology, 2020, 15, 86.	2.7	21
26	Macrophage-Derived Extracellular Vesicle Promotes Hair Growth. Cells, 2020, 9, 856.	4.1	60
27	F-18 FDG PET for assessment of disease activity of large vessel vasculitis: A systematic review and meta-analysis. Journal of Nuclear Cardiology, 2019, 26, 59-67.	2.1	31
28	Susceptibility of the Index Urinary Tract Infection to Prophylactic Antibiotics Is a Predictive Factor of Breakthrough Urinary Tract Infection in Children with Primary Vesicoureteral Reflux Receiving Continuous Antibiotic Prophylaxis. Journal of Korean Medical Science, 2019, 34, e156.	2.5	5
29	Enhancing prognosis prediction using pre-treatment nodal SUVmax and HPV status in cervical squamous cell carcinoma. Cancer Imaging, 2019, 19, 43.	2.8	8
30	Clinical outcomes of patients with T4 or N1b well-differentiated thyroid cancer after different strategies of adjuvant radioiodine therapy. Scientific Reports, 2019, 9, 5570.	3.3	12
31	Combination Treatment with the <i>BRAF<sup>V600E</sup></i> Inhibitor Vemurafenib and the BH3 Mimetic Navitoclax for <i>BRAF</i> -Mutant Thyroid Carcinoma. Thyroid, 2019, 29, 540-548.	4.5	13
32	A systematic review and meta-analysis of 18F-fluorodeoxyglucose positron emission tomography or positron emission tomography/computed tomography for detection of infected prosthetic vascular grafts. Journal of Vascular Surgery, 2019, 70, 307-313.	1.1	24
33	The ability of whole-body SUVmax in F-18 FDG PET/CT to predict suboptimal cytoreduction during primary debulking surgery for advanced ovarian cancer. Journal of Ovarian Research, 2019, 12, 12.	3.0	15
34	The Preventive Effect of Parotid Gland Massage on Salivary Gland Dysfunction During High-Dose Radioactive Iodine Therapy for Differentiated Thyroid Cancer. Clinical Nuclear Medicine, 2019, 44, 625-633.	1.3	18
35	Serum thyroglobulin elevation after needle aspiration of the lymph nodes: the predictive value for detecting metastasis in papillary thyroid cancer patients – a pilot study. Medicine (United States), 2019, 98, e16461.	1.0	4
36	Enhancement of antitumor potency of extracellular vesicles derived from natural killer cells by IL-15 priming. Biomaterials, 2019, 190-191, 38-50.	11.4	87

#	Article	IF	CITATIONS
37	Updates of Radioiodine Treatment for Graves' Disease. International Journal of Thyroidology, 2019, 12, 85.	0.1	0
38	Prediction of Advanced Axillary Lymph Node Metastases (ypN2-3) Using Breast MR imaging and PET/CT after Neoadjuvant Chemotherapy in Invasive Ductal Carcinoma Patients. Scientific Reports, 2018, 8, 3181.	3.3	9
39	Amyloid Deposits and Idiopathic Normal-Pressure Hydrocephalus: An 18F-Florbetaben Study. European Neurology, 2018, 79, 192-199.	1.4	5
40	Prognostic significance of residual lymph node status after definitive chemoradiotherapy in patients with node-positive cervical cancer. Gynecologic Oncology, 2018, 148, 449-455.	1.4	8
41	PEGylated crushed gold shell-radiolabeled core nanoballs for in vivo tumor imaging with dual positron emission tomography and Cerenkov luminescent imaging. Journal of Nanobiotechnology, 2018, 16, 41.	9.1	27
42	Predictive value of cortical transit time on MAG3 for surgery in antenatally detected unilateral hydronephrosis caused by ureteropelvic junction stenosis. Journal of Pediatric Urology, 2018, 14, 55.e1-55.e6.	1.1	17
43	Optimization of Dendritic Cell-Mediated Cytotoxic T-Cell Activation by Tracking of Dendritic Cell Migration Using Reporter Gene Imaging. Molecular Imaging and Biology, 2018, 20, 398-406.	2.6	6
44	Prognostic value of 18F-fluorodeoxyglucose bone marrow uptake in patients with solid tumors. Medicine (United States), 2018, 97, e12859.	1.0	8
45	New Optical Imaging Reporter-labeled Anaplastic Thyroid Cancer-Derived Extracellular Vesicles as a Platform for In Vivo Tumor Targeting in a Mouse Model. Scientific Reports, 2018, 8, 13509.	3.3	17
46	A New Approach for Loading Anticancer Drugs Into Mesenchymal Stem Cell-Derived Exosome Mimetics for Cancer Therapy. Frontiers in Pharmacology, 2018, 9, 1116.	3.5	179
47	Diagnostic performance of HMGA2 gene expression for differentiation of malignant thyroid nodules: A systematic review and metaâ€analysis. Clinical Endocrinology, 2018, 89, 856-862.	2.4	1
48	Migration of mesenchymal stem cells to tumor xenograft models and <i>in vitro</i> drug delivery by doxorubicin. International Journal of Medical Sciences, 2018, 15, 1051-1061.	2.5	45
49	Regulated Mesenchymal Stem Cells Mediated Colon Cancer Therapy Assessed by Reporter Gene Based Optical Imaging. International Journal of Molecular Sciences, 2018, 19, 1002.	4.1	16
50	Prevalence and Risk Factors of Atypical Femoral Fracture Bone Scintigraphic Feature in Patients Experiencing Bisphosphonate-Related Osteonecrosis of the Jaw. Nuclear Medicine and Molecular Imaging, 2018, 52, 311-317.	1.0	2
51	Targeting and Therapy of Clioblastoma in a Mouse Model Using Exosomes Derived From Natural Killer Cells. Frontiers in Immunology, 2018, 9, 824.	4.8	77
52	Risk factors for radioactive iodine-avid metastatic lymph nodes on post I-131 ablation SPECT/CT in low- or intermediate-risk groups of papillary thyroid cancer. PLoS ONE, 2018, 13, e0202644.	2.5	8
53	In vivo Non-invasive Imaging of Radio-Labeled Exosome-Mimetics Derived From Red Blood Cells in Mice. Frontiers in Pharmacology, 2018, 9, 817.	3.5	72
54	Novel alternatives to extracellular vesicle-based immunotherapy – exosome mimetics derived from natural killer cells. Artificial Cells, Nanomedicine and Biotechnology, 2018, 46, 166-179.	2.8	74

#	Article	IF	CITATIONS
55	Multimodality Imaging of Bone Marrow–Derived Dendritic Cell Migration and Antitumor Immunity. Translational Oncology, 2017, 10, 262-270.	3.7	14
56	Clinical outcomes of low-dose and high-dose postoperative radioiodine therapy in patients with intermediate-risk differentiated thyroid cancer. Nuclear Medicine Communications, 2017, 38, 228-233.	1.1	27
57	Development of an athyroid mouse model using 1311 ablation after preparation with a low-iodine diet. Scientific Reports, 2017, 7, 13284.	3.3	7
58	Non-invasive visualization of mast cell recruitment and its effects in lung cancer by optical reporter gene imaging and glucose metabolism monitoring. Biomaterials, 2017, 112, 192-203.	11.4	5
59	Visualization of Macrophage Recruitment to Inflammation Lesions using Highly Sensitive and Stable Radionuclide-Embedded Gold Nanoparticles as a Nuclear Bio-Imaging Platform. Theranostics, 2017, 7, 926-934.	10.0	29
60	Natural Killer Cell (NK-92MI)-Based Therapy for Pulmonary Metastasis of Anaplastic Thyroid Cancer in a Nude Mouse Model. Frontiers in Immunology, 2017, 8, 816.	4.8	44
61	In Vivo Tracking of Chemokine Receptor CXCR4-Engineered Mesenchymal Stem Cell Migration by Optical Molecular Imaging. Stem Cells International, 2017, 2017, 1-10.	2.5	60
62	Prognostic value of intratumoral metabolic heterogeneity on F-18 fluorodeoxyglucose positron emission tomography/computed tomography in locally advanced cervical cancer patients treated with concurrent chemoradiotherapy. Oncotarget, 2017, 8, 90402-90412.	1.8	21
63	Pathological N1b Node Metastasis Itself Can Be Still a Valid Prognostic Factor in PTC after High Dose RAI Therapy. International Journal of Thyroidology, 2016, 9, 159.	0.1	2
64	Visualization of the Biological Behavior of Tumor-Associated Macrophages in Living Mice with Colon Cancer Using Multimodal Optical Reporter Gene Imaging. Neoplasia, 2016, 18, 133-141.	5.3	21
65	Combined Positron Emission Tomography and Cerenkov Luminescence Imaging of Sentinel Lymph Nodes Using PEGylated Radionuclideâ€Embedded Gold Nanoparticles. Small, 2016, 12, 4894-4901.	10.0	34
66	Radionuclide-embedded gold nanoparticles for enhanced dendritic cell-based cancer immunotherapy, sensitive and quantitative tracking of dendritic cells with PET and Cerenkov luminescence. NPG Asia Materials, 2016, 8, e281-e281.	7.9	51
67	Inverse Agonist of Estrogen-Related Receptor Î <sup>3</sup> Enhances Sodium Iodide Symporter Function Through Mitogen-Activated Protein Kinase Signaling in Anaplastic Thyroid Cancer Cells. Journal of Nuclear Medicine, 2015, 56, 1690-1696.	5.0	38
68	Neurolymphomatosis on F-18 FDG PET/CT and MRI Findings: A Case Report. Nuclear Medicine and Molecular Imaging, 2011, 45, 76-78.	1.0	23
69	Prognostic Value of Primary Tumor Uptake on F-18 FDG PET/CT in Patients with Invasive Ductal Breast Cancer. Nuclear Medicine and Molecular Imaging, 2011, 45, 117-124.	1.0	44
70	Incidental pituitary uptake on whole-body 18F-FDG PET/CT: a multicentre study. European Journal of Nuclear Medicine and Molecular Imaging, 2010, 37, 2334-2343.	6.4	69
71	False-Positive Axillary Lymph Node on F-18 FDG PET/CT due to Moxibustion Therapy. Nuclear Medicine and Molecular Imaging, 2010, 44, 307-308.	1.0	0
72	Improved Detection of Lung or Bone Metastases with an I-131 Whole Body Scan on the 7th Day After High-Dose I-131 Therapy in Patients with Thyroid Cancer. Nuclear Medicine and Molecular Imaging, 2010, 44, 273-281.	1.0	26